

# Rational Design of a Structural Framework with Potential Use to Develop Chemical Reagents That Target and Modulate Multiple Facets of Alzheimer's Disease

Sanghyun Lee,<sup>†,Δ</sup> Xueyun Zheng,<sup>‡</sup> Janarthanan Krishnamoorthy,<sup>§,⊥</sup> Masha G. Savelieff,<sup>†</sup> Hyun Min Park,<sup>†,¶</sup> Jeffrey R. Brender,<sup>§,⊥</sup> Jin Hoon Kim,<sup>†,¶</sup> Jeffrey S. Derrick,<sup>⊥</sup> Akiko Kochi,<sup>⊥</sup> Hyuck Jin Lee,<sup>⊥</sup> Cheal Kim,<sup>¶</sup> Ayyalusamy Ramamoorthy,<sup>\*,§,⊥</sup> Michael T. Bowers,<sup>\*,‡</sup> and Mi Hee Lim<sup>\*,†,⊥,||</sup>

<sup>†</sup>Life Sciences Institute, University of Michigan, Ann Arbor, Michigan 48109-2216, United States

<sup>‡</sup>Department of Chemistry and Biochemistry, University of California, Santa Barbara, California 93106-9510, United States

<sup>§</sup>Biophysics, University of Michigan, Ann Arbor, Michigan 48109-1055, United States

<sup>⊥</sup>Department of Chemistry, University of Michigan, Ann Arbor, Michigan 48109-1055, United States

<sup>¶</sup>Department of Chemistry, Seoul National University of Science and Technology, Seoul 139-743, Korea

<sup>||</sup>School of Nano-Bioscience and Chemical Engineering, Ulsan National Institute of Science and Technology (UNIST), Ulsan 689-798, Korea

## Supporting Information

**ABSTRACT:** Alzheimer's disease (AD) is characterized by multiple, intertwined pathological features, including amyloid- $\beta$  ( $A\beta$ ) aggregation, metal ion dyshomeostasis, and oxidative stress. We report a novel compound (ML) prototype of a rationally designed molecule obtained by integrating structural elements for  $A\beta$  aggregation control, metal chelation, reactive oxygen species (ROS) regulation, and antioxidant activity within a single molecule. Chemical, biochemical, ion mobility mass spectrometric, and NMR studies indicate that the compound ML targets metal-free and metal-bound  $A\beta$  (metal- $A\beta$ ) species, suppresses  $A\beta$  aggregation in vitro, and diminishes toxicity induced by  $A\beta$  and metal-treated  $A\beta$  in living cells. Comparison of ML to its structural moieties (i.e., 4-(dimethylamino)phenol (DAP) and (8-aminoquinolin-2-yl)methanol (1)) for reactivity with  $A\beta$  and metal- $A\beta$  suggests the synergy of incorporating structural components for both metal chelation and  $A\beta$  interaction. Moreover, ML is water-soluble and potentially brain permeable, as well as regulates the formation and presence of free radicals. Overall, we demonstrate that a rational structure-based design strategy can generate a small molecule that can target and modulate multiple factors, providing a new tool to uncover and address AD complexity.



Alzheimer's disease (AD) is characterized by a loss of brain function which affects memory, cognition, and behavior.<sup>1</sup> Development of a cure for AD has been hindered by a lack of understanding of both the causes and mechanisms of disease onset and progression.<sup>2-6</sup> The AD brain exhibits several characteristic pathological features, such as accumulation of misfolded amyloid- $\beta$  ( $A\beta$ ), metal ion dyshomeostasis, and elevated oxidative stress.<sup>3-12</sup> Two amyloidogenic peptides,  $A\beta$ 40 and  $A\beta$ 42, present in the brain at ca. 90% and 9%, respectively, are primarily produced upon cleavage of amyloid precursor protein (APP) by  $\beta$ - and  $\gamma$ -secretases.<sup>3-6</sup> Both peptides tend to aggregate, generating oligomers and fibrils.<sup>3-6,8,12,13</sup> Although  $A\beta$  is proposed to be a causative agent in AD, a relationship between specific peptide oligomers and toxicity remains unclear despite recent findings indicating soluble  $A\beta$  oligomers as possible neurotoxic species.<sup>3-6,8,12-15</sup>

In addition to  $A\beta$  imbalance, high levels of metal ions (Cu, ca. 0.4 mM; Zn, ca. 1 mM; Fe, ca. 0.9 mM) have been found in  $A\beta$  plaques of AD brains.<sup>3,5-12</sup> These metals, particularly Cu and Zn, bind to  $A\beta$  peptides facilitating their aggregation. Moreover, dysregulated redox active metal ions, Cu(I/II) and Fe(II/III), both unbound and bound to  $A\beta$  peptides, are observed to promote overproduction of reactive oxygen species (ROS) that damage biological molecules, such as proteins, DNA, and lipids.<sup>3,5-12,16-18</sup> Overall, because of the involvement of numerous factors (e.g., metal-free/-associated  $A\beta$  species, metals, free radicals) and their potential intercon-

Received: September 29, 2013

Published: December 27, 2013

tion in AD pathogenesis, the causative agents in this multifaceted disease remain to be unambiguously identified.

Chemical reagents to target and regulate these multiple factors in AD are desirable to advance our understanding of AD complexity and offer possible answers for remediation. Toward this effort, small molecules have been developed via a rational structure-based incorporation approach by integrating an  $A\beta$  interacting framework with a metal chelation moiety into a single molecule designed to target and modulate metal-associated  $A\beta$  (metal- $A\beta$ ) species.<sup>8,9,12,18–26</sup> These compounds were observed to control metal-induced  $A\beta$  aggregation, attenuate ROS formation by metal- $A\beta$ , or regulate metal- $A\beta$  toxicity in vitro and in living cells.<sup>21–26</sup> In addition, interaction and reactivity of natural products, such as the green tea extract, (–)-epigallocatechin-3-gallate, and myricetin, with metal- $A\beta$  species have also been investigated showing distinct reactivity with metal- $A\beta$  over metal-free  $A\beta$ .<sup>27,28</sup> To the best of our knowledge, however, a single designed compound, targeting all these factors (i.e.,  $A\beta$ , metal- $A\beta$ , metal ions, free radicals, Figure 1) and regulating their reactivities, has not been reported to date.

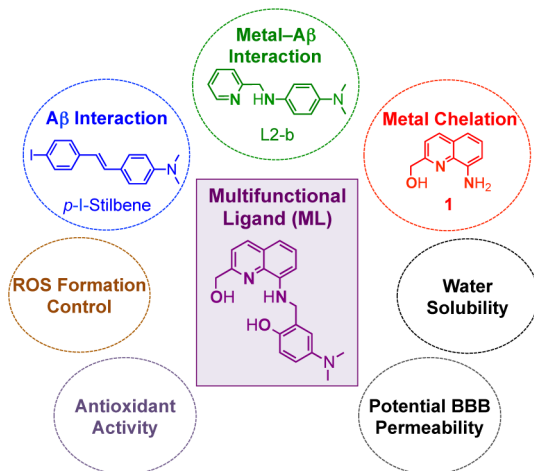


**Figure 1.** Rational structure-based design principle (incorporation approach) of a multifunctional ligand (ML). Atoms responsible for metal binding are in bold. Chemical structures: ML = 4-(dimethylamino)-2-(((2-(hydroxymethyl)quinolin-8-yl)-amino)-methyl)phenol; *p*-I-stilbene = (*E*)-4-(4-iodostyryl)-*N,N*-dimethylaniline; L2-b = *N*<sup>1</sup>,*N*<sup>1</sup>-dimethyl-*N*<sup>1</sup>-(pyridin-2-ylmethyl)benzene-1,4-diamine; **1** = (8-aminoquinolin-2-yl)methanol.

Herein, we present a novel ligand (ML) as the first example of a rationally designed molecule to afford multiple properties

within a single entity (Figure 1). Our investigations of ML's activity toward  $A\beta$ , metal- $A\beta$ , metal ions, and free radicals, as well as its potential blood-brain barrier (BBB) permeability confirm that careful selection and consideration of molecular properties can result in the design of a molecule to target and modulate multiple pathological features of AD. The compound **1** (Figure 1 for structure), without an  $A\beta$  interacting moiety, was also studied in parallel to demonstrate that ML's reactivity toward  $A\beta$  and metal- $A\beta$  could arise from the synergy of its metal chelation and  $A\beta$  interaction properties.

## RESULTS AND DISCUSSION

**Design Consideration for a Multifunctional Ligand (ML).** To develop a chemical tool capable of both targeting and modulating the reactivity of multiple AD pathological factors in biological systems, we designed a novel molecule (ML) with the potential for interaction with  $A\beta$  and metal- $A\beta$ , metal chelation, control of ROS generation, antioxidant activity, water solubility, and BBB permeability (Figure 1). For  $A\beta$ /metal- $A\beta$  interactions and metal chelation, ML was constructed by combining *p*-I-stilbene, a known  $A\beta$  imaging agent,<sup>29</sup> with L2-b, a molecule previously reported to target and regulate metal- $A\beta$ <sup>22</sup> and **1**, a metal chelator<sup>30</sup> (Figure 1). For enhanced metal binding properties, an additional hydroxyl group, along with nitrogen and oxygen donor atoms from **1**, was incorporated into ML affording a tetradentate ligand for Cu(II) with 1:1 metal-to-ligand stoichiometry.<sup>30</sup> ML was constructed to accommodate a slightly distorted square planar geometry for Cu(II) similar to 2-[(8-quinolinylamino)methyl]phenol.<sup>30</sup> In this conformation, the ligand cannot easily accommodate the preferred tetrahedral geometry of Cu(I) for redox cycles of Cu(I/II) and, thus, is able to inhibit ROS generation. For antioxidant activity, substituents (i.e., both quinoline and phenolic groups, Figure 1)<sup>31–33</sup> known to have antioxidant capability were integrated into ML. Lastly, polar functionalities (e.g., hydroxyl and amino groups) were introduced into the backbone for water solubility. All structural elements were selected to adhere to values of Lipinski's rules and logBB for possible drug-likeness and BBB penetration (Table 1).<sup>22,25,34,35</sup> ML was synthesized by modifications to previously reported procedures (Schiff base condensation followed by reduction of imine to amine, ca. 50% yield) as shown in Scheme 1.<sup>30</sup>

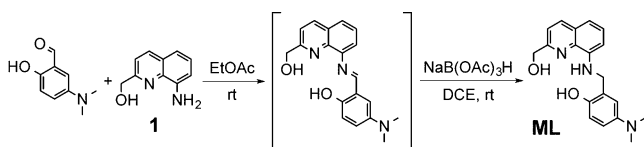
**Direct Interactions of ML with Soluble Forms of  $A\beta$  and Metal- $A\beta$ .** To determine whether ML binds to  $A\beta$ 40 and  $A\beta$ 42, mixtures of the compound with either peptide were first monitored by mass spectrometry (MS). In the mass spectrum of a 1:5 mixture of  $A\beta$ 42 and ML (Figure 2a), there were three peaks representing  $A\beta$ 42 with charge (*z*) to oligomer number (*n*) ratio  $z/n = -4, -3,$  and  $-5/2$ , similar to the mass spectrum

**Table 1.** Values (MW, *clogP*, HBA, HBD, PSA, logBB, and  $-\log P_e$ )<sup>a</sup> for ML and **1**

Compound	MW	<i>clogP</i>	HBA	HBD	PSA (Å)	logBB	$-\log P_e$	CNS± prediction <sup>b</sup>
ML	323	2.57	5	3	68.1	-0.478	4.49 (±0.01)	CNS+
<b>1</b>	174	0.889	3	3	58.6	-0.593	4.70 (±0.01)	CNS+
Lipinski's rules and others	≤ 450	≤ 5.0	≤ 10	≤ 5	≤ 90	> 3.0 (readily); < -1.0 (poorly)	< 5.4; > 5.7	CNS+; CNS-

<sup>a</sup>MW, molecular weight; *clogP*, calculated logarithm of the octanol-water partition coefficient; HBA, hydrogen bond acceptor atoms; HBD, hydrogen bond donor atoms; PSA, polar surface area; logBB =  $-0.0148 \times \text{PSA} + 0.152 \times \text{clogP} + 0.139$  (logBB > 3.0, readily crosses BBB; logBB < -1.0, poorly distributed to the brain);  $-\log P_e$  values were determined using the Parallel Artificial Membrane Permeability Assay (PAMPA), and average  $-\log P_e$  values were then calculated by the PAMPA 9 Explorer software v. 3.5. <sup>b</sup>Prediction of a compound's ability to penetrate the central nervous system (CNS) on the basis of literature values. Compounds categorized as CNS+ possess the ability to penetrate the BBB and are available in the CNS. Compounds assigned as CNS- have poor permeability through the BBB; therefore, their bioavailability into the CNS is considered to be minimal.

## Scheme 1. Synthetic Route to ML



of pure  $A\beta_{42}$  without **ML** (Figure 2b). Moreover, there were two tailing peaks ( $m/z = 1611.3$  and  $1718.7$ , respectively) corresponding to  $z/n = -3$  complexes of  $A\beta_{42}$  with one and two **ML** molecules bound, respectively. In the mass spectrum of the mixture of  $A\beta_{40}$  and **ML** (Supporting Information Figure S1), a tailing peak indicating to the  $z/n = -3$  complex of  $A\beta_{40}$  and **ML** was also observed. These results suggest that **ML** can directly bind to both  $A\beta_{40}$  and  $A\beta_{42}$  with either a 1:1 or 1:2  $A\beta$ :**ML** stoichiometry.

Direct binding of **ML** to monomeric  $A\beta_{40}$  was supported by NMR experiments, which showed either a small but detectable broadening or a chemical shift change for freshly prepared  $A\beta_{40}$  with a stoichiometric amount of **ML**, particularly for  $A\beta$  residues F4, R5, V12, and Q15 (Figure 2c–f). These residues form an apparent binding pocket in the aqueous NMR structure of  $A\beta_{40}$  (Figure 2f).<sup>36</sup> Larger changes in chemical shift were observed with an excess of **ML** possibly due to a change in the conformation or oligomerization state of  $A\beta_{40}$  at this concentration of **ML** (Figure 2d). The chemical shift of methionine 35 (M35) did not change appreciably, indicating that **ML** does not cause oxidation of  $A\beta_{40}$ .<sup>37</sup>

To investigate the interaction of **ML** with metal-bound  $A\beta$ , samples of  $\text{Cu(II)}-A\beta_{40/42}$  or  $\text{Zn(II)}-A\beta_{40/42}$  with and without **ML** were analyzed by MS (Figure 2g and h; Supporting Information Figures S2 and S3). The mass spectrum of a 1:1 mixture of  $A\beta_{42}$  and  $\text{Cu(II)}$  without **ML** displayed two sets of

peaks for each charge state  $z/n = -4$ ,  $-3$ , and  $-5/2$ , corresponding to  $A\beta_{42}$  with one and two  $\text{Cu(II)}$  binding, respectively (Figure 2h). When **ML** was added to preincubated  $\text{Cu(II)}-A\beta_{42}$ , a mixture of species was observed (Figure 2g). In addition to the peaks observed in **ML**-free samples corresponding to  $A\beta_{42}$  with one or two  $\text{Cu(II)}$ , three additional peaks representing metal-free  $A\beta_{42}$  with  $z/n = -4$ ,  $-3$ , and  $-5/2$  were also detected, indicating that **ML** can competitively chelate  $\text{Cu(II)}$  from  $A\beta_{42}$ . Note that peak intensities of  $A\beta_{42}$  with two  $\text{Cu(II)}$  bound decreased dramatically upon **ML** addition. A tailing peak corresponding to a complex of  $A\beta_{42}$  with one **ML** bound was observed. Moreover, peaks indicating complexes of  $A\beta_{42}$ , **ML**, and one or two  $\text{Cu(II)}$  ( $m/z = 1633$  and  $1653$ , respectively) were present, indicating **ML** bound to  $A\beta_{42}$  and metal- $A\beta_{42}$ .

Similar to  $A\beta_{42}$ , the mass spectrum of preincubated  $\text{Cu(II)}-A\beta_{40}$  treated with **ML** displayed peaks indicative of both  $A\beta_{40}-\text{Cu(II)}-\text{ML}$  ternary complexes and copper-liberated  $A\beta_{40}$  (Supporting Information Figure S2).  $\text{Zn(II)}$ -associated  $A\beta_{40/42}$  were also investigated with **ML**. The mass spectrum of a 1:1:2 mixture of  $A\beta_{40/42}:\text{Zn(II)}:\text{ML}$  showed peaks corresponding to  $A\beta_{40/42}-\text{Zn(II)}-\text{ML}$  complexes ( $z/n = -3$  and  $-5/2$ ) as well as slight increased intensity of peaks corresponding to metal-free  $A\beta$  compared to those without **ML** (Supporting Information Figure S3). Overall, these results indicate that **ML** not only forms complexes with both  $\text{Cu(II)}-A\beta$  and  $\text{Zn(II)}-A\beta$  but also competitively chelates metal ions from metal- $A\beta$  generating metal-free  $A\beta$  species.

**Interactions of ML with  $A\beta$  Fibers.** To probe the interaction of **ML** with larger aggregates, we measured the interaction of **ML** with metal-free  $A\beta_{40}$  fibers by  $^1\text{H}$  NMR (Figure 3a). Even at low fiber concentrations ( $A\beta_{40}:\text{ML}$ , 1:10), chemical shift perturbations were detected within the quinoline

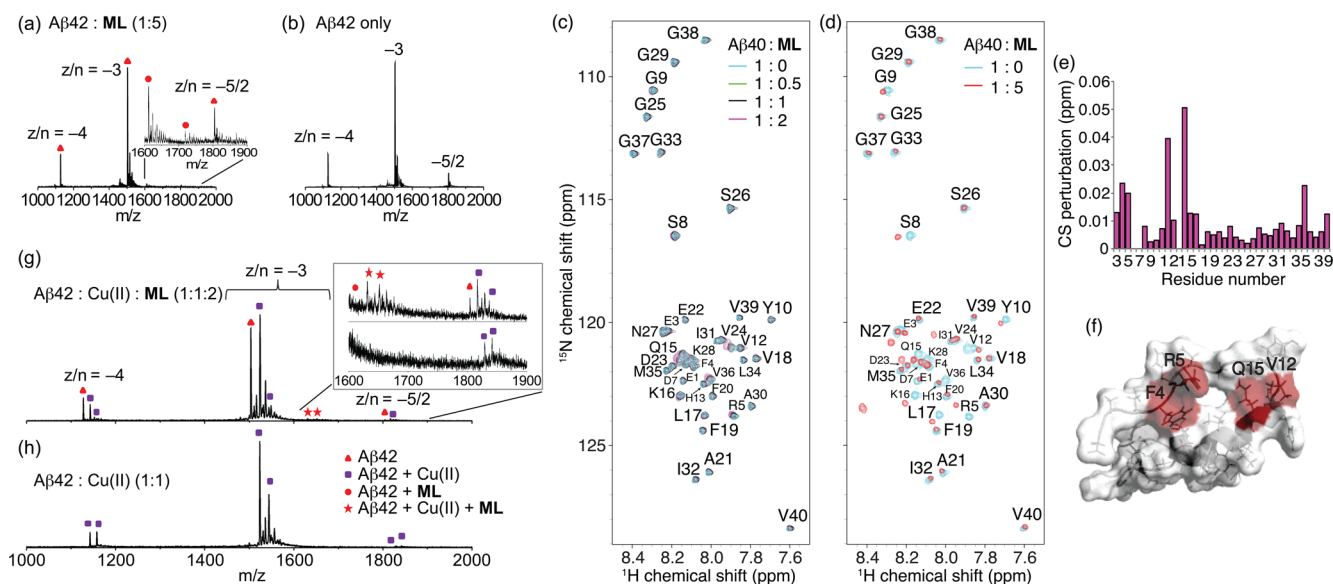


**Figure 2.** Interactions of **ML** with soluble metal-free or  $\text{Cu(II)}$ -treated  $A\beta$  species monitored by mass spectrometry or SOFAST-HMQC NMR. Mass spectra of (a) 1:5 mixture of  $A\beta_{42}$  and **ML** and (b) pure  $A\beta_{42}$  ( $z/n = \text{charge/oligomer number}$ ). (c and d) 2D SOFAST-HMQC NMR spectra of **ML**-titrated metal-free monomeric  $A\beta_{40}$ . Freshly dissolved  $A\beta_{40}$  ( $80 \mu\text{M}$ ) in  $50 \text{ mM}$  Tris-DCI (pD 7.3) was titrated to (c)  $40\text{--}160 \mu\text{M}$  or (d)  $400 \mu\text{M}$  **ML** at  $4 \text{ }^\circ\text{C}$ . The contour level of (d) has been adjusted to clearly show ligand-bound resonances. (e) Chemical shift perturbations within  $A\beta_{40}$  following addition of **ML** ( $A\beta:\text{ML} = 1:2$ ). (f) Residues with largest changes in chemical shift at 1:1  $A\beta_{40}:\text{ML}$  mapped onto the NMR structure of the helical conformer of the  $A\beta_{40}$  structural ensemble (PDB 2LFM). Mass spectra of (g)  $A\beta_{42}$ ,  $\text{Cu(II)}$ , and **ML** (1:1:2) and of (h)  $A\beta_{42}$  and  $\text{Cu(II)}$  (1:1). Peaks for pure  $A\beta_{42}$ ,  $\text{Cu(II)}$ -bound  $A\beta_{42}$ , **ML**-bound  $A\beta_{42}$ , and  $A\beta_{42}-\text{Cu(II)}-\text{ML}$  complexes are noted with triangles, rectangles, circles, and stars, respectively.

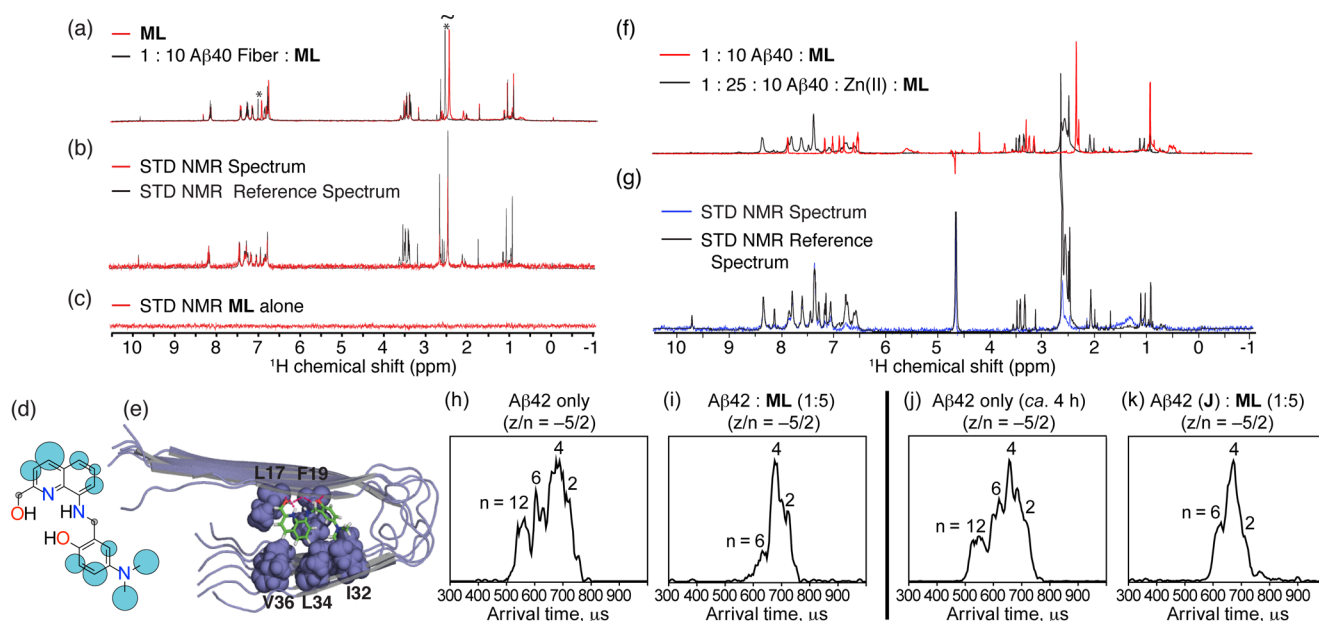


**Figure 3.** (a–g) Interaction of ML with fibrillar  $A\beta_{40}$  species by saturation transfer difference (STD) NMR and (h–k) influence of ML on early  $A\beta_{42}$  oligomerization monitored by mass spectrometry and ion mobility studies. (a) Chemical shift changes in the  $^1\text{H}$  spectra of ML upon the addition of 10 mol % metal-free  $A\beta_{40}$  fibers in 100%  $\text{D}_2\text{O}$  (20 mM deuterated Tris–DCl, pD 7.4). Large chemical shift changes can be seen in the aniline ring and dimethylamino groups (marked with an asterisk). (b)  $^1\text{H}$  STD NMR spectra of ML with  $A\beta_{40}$  fibers ( $A\beta$ :ML = 1:10). Comparison of STD signal intensity (red) to the STD reference (black) reflects the relative proximity of the corresponding proton to the  $A\beta_{40}$  fiber. (c)  $^1\text{H}$  STD NMR spectra of ML alone showing the absence of an STD signal in the absence of  $A\beta_{40}$  fibers. (d) Normalized STD intensities mapped to ML's structure. Larger blue circles indicate a more intense STD effect; gray circles indicate the absence of an STD signal. (e) Lowest energy docked conformation of ML to  $A\beta_{40}$  fibers (PDB 2LMO). Other docked conformations and a cluster analysis can be found in Supporting Information Figures S4 and S5. (f) Comparison of the  $^1\text{H}$  spectra of ML (200  $\mu\text{M}$ ) with  $A\beta_{40}$  fibers (20  $\mu\text{M}$ ) in 100%  $\text{D}_2\text{O}$  (20 mM deuterated Tris–DCl, pD 7.4) with (black) and without (red) 500  $\mu\text{M}$   $\text{ZnCl}_2$ . The large chemical shift changes are evidence of binding of  $\text{Zn}(\text{II})$  to ML. (g)  $^1\text{H}$  STD NMR spectra of ML with  $A\beta_{40}$  fibers in a ratio of 10:1 in the presence of  $\text{ZnCl}_2$  (500  $\mu\text{M}$ ). Arrival time distributions (ATDs) for the  $z/n = -5/2$  peak of (h) pure  $A\beta_{42}$  and (i) 1:5 mixture of  $A\beta_{42}$  and ML sample, respectively. (j) ATD for the  $-5/2$  peak of the  $A\beta_{42}$  sample prepared and placed on ice for ca. 4 h. (k) ATD for the  $-5/2$  peak of the preincubated  $A\beta_{42}$  sample immediately following the addition of ML (ca. 5 min).

and aniline rings and for the dimethylamino group of ML. The monomeric  $A\beta$  signal was not observed, indicating that ML does not completely convert metal-free  $A\beta$  fibers into the monomeric form, in agreement with results from aggregation experiments (vide infra). The interaction of ML with  $A\beta_{40}$  fibers was probed more directly by saturation transfer difference (STD) NMR experiments (Figure 3b and c). Signals in STD NMR are proportional to the proximity of each ligand atom to its macromolecular binding partner, allowing atomic-level mapping of ligand binding interactions to be made.<sup>38</sup> Relatively strong saturation effects can be seen throughout ML (Figure 3d), suggesting that it can pack tightly against fibers. This binding mode is supported by docking simulations (Figure 3e and Supporting Information Figures S4 and S5) showing intimate interaction of ML with the side-chains and backbone of the unpaired  $\beta$  sheet at the end of the  $A\beta$  fiber. The lowest energy conformations were stabilized by hydrogen bonding of the hydroxyl and amino moieties of ML to the peptide backbone,  $\pi$ – $\pi$  stacking of ML's quinoline ring with the phenyl ring of F19, and Van der Waals interactions of ML's dimethylamino group with the side chains of I32 and L34 on the opposing  $\beta$  sheet (Figure 3e and Supporting Information Figures S4 and S5). Preservation of Van der Waals interactions between the dimethylamino moiety and  $A\beta$  fibers suggests that this structural group in a meta position to the bridgehead could also be effective for  $A\beta$  interaction compared to that in a para position, as for *p*-I-stilbene (Figure 1).<sup>29</sup> In this conformation, most of ML was in contact with the fiber with the exception of

the bridge-head  $\text{CH}_2$ , in agreement with the STD results. Some features of the  $A\beta$  fiber–ML interaction were dependent on the specific  $A\beta$  fiber model used in the simulations and also varied among the low energy conformations obtained for each model (Supporting Information Figures S4 and S5). In docking investigations, ML would consistently intercalate between the “steric zipper” of the exposed  $\beta$  strands at the end of the  $A\beta$  fiber, most likely disrupting the potential hydrogen bonding network for incoming  $A\beta_{40}$  monomers and preventing fiber extension. Strong chemical shift perturbations in ML upon treatment with  $\text{Zn}(\text{II})$  in the presence of  $A\beta_{40}$  fibers demonstrate that ML interacts with  $\text{Zn}(\text{II})$  (Figure 3f), as confirmed by metal binding studies (vide infra). STD NMR of  $\text{Zn}(\text{II})$ – $A\beta_{40}$  fibers showed a similar saturation pattern (Figure 3g) as the metal-free samples (Figure 3b) but with reduced intensity, indicating that ML could bind to  $\text{Zn}(\text{II})$ – $A\beta$  fibers in a similar manner, although somewhat less effectively.

**Metal Binding Properties of ML.**  $\text{Cu}(\text{II})$  and  $\text{Zn}(\text{II})$  binding to ML was measured by UV–visible (UV–vis) spectroscopy (Supporting Information Figure S6). Upon addition of one equivalent of  $\text{CuCl}_2$  or  $\text{ZnCl}_2$  to a solution of ML at pH 7.4, a new absorption band at ca. 457 nm (for  $\text{CuCl}_2$ ) or ca. 450 nm (for  $\text{ZnCl}_2$ ) was observed, indicative of metal binding to the ligand. Moreover, ML's selectivity toward  $\text{Cu}(\text{II})$  or  $\text{Zn}(\text{II})$  over other biologically relevant divalent metal ions [ $\text{Mg}(\text{II})$ ,  $\text{Ca}(\text{II})$ ,  $\text{Mn}(\text{II})$ ,  $\text{Fe}(\text{II})$ ,  $\text{Co}(\text{II})$ , and  $\text{Ni}(\text{II})$ ] was investigated by competition experiments. ML was bound to  $\text{Cu}(\text{II})$  selectively, even at 20-fold higher concentrations (1

mM) of other divalent ions (Supporting Information Figure S7). **ML** was shown to be relatively selective for Zn(II) over Mg(II), Ca(II), or Mn(II) at stoichiometric ratios, whereas it could not bind Zn(II) over Fe(II), Co(II), Ni(II), or Cu(II). **ML** could interact with Zn(II) over excess Mg(II) and Ca(II) (Supporting Information Figure S7). Metal binding and Cu(II) selectivity of **1** (see Figure 1 for structure) were also confirmed (Supporting Information Figure S7).

Solution speciation and metal binding affinities of **ML** were determined by UV-vis variable-pH (2–8) titration experiments. Three acidity constants ( $pK_a$ ) were obtained (2.628, 3.971, and 6.230), suggesting the presence of mono-, di-, and triprotonated ligand forms in the pH range of 2–8 (Supporting Information Figure S8). The solution speciation diagram based on the acidity constants indicates that **ML** exists mainly in neutral form (ca. 94%) at physiological pH (i.e., 7.4). Stability constants for **ML** with Cu(II) and Zn(II) were identified by solution speciation studies of Cu(II)–**ML** and Zn(II)–**ML** complexes. Dissociation constants ( $K_d$ ) for **ML** with Cu(II) (picomolar range) and Zn(II) (nanomolar range) based on concentrations of unchelated Cu(II) or Zn(II) at pH 7.4 (Supporting Information Figure S8) demonstrate that **ML** coordinates Cu(II) more strongly than Zn(II). **ML** chelates Cu(II) and Zn(II) more effectively than **1** (micromolar range for both metal ions, pH 7.4; Supporting Information Figure S9) and preferentially forms 1:1 metal:**ML** complexes, whereas **1** generates a mixture of 1:1 and 1:2 complexes of metal:**1**. Moreover,  $K_d$  of **ML** values for Cu(II) and Zn(II) are comparable to those of Cu(II)–**A $\beta$**  (picomolar to nanomolar) and Zn(II)–**A $\beta$**  (nanomolar to micromolar),<sup>5–9,12,16–18</sup> implying that **ML** could interact with metal ions surrounded by soluble **A $\beta$**  species, which supports the outcomes from MS (vide supra) and reactivity studies with metal–**A $\beta$**  species (vide infra).

#### Modulation of the Early Oligomerization of **A $\beta$** by **ML**.

Ion mobility–mass spectrometry (IM–MS)<sup>39</sup> was employed to investigate the influence of **ML** on early **A $\beta$**  aggregation. IM–MS is capable of separating species with the same mass-to-charge ratio, but different oligomer conformations and sizes, and has been successfully applied to studying **A $\beta$**  structure and screening for small molecule inhibitors of **A $\beta$**  aggregation.<sup>40–43</sup> The arrival time distributions (ATDs) for **A $\beta$ 42** peaks at  $z/n = -5/2$  with and without **ML** are shown in Figures 3h–k. The ATD of the  $-5/2$  peak of **A $\beta$ 42** without **ML** (Figure 3h) exhibited four features with arrival times at ca. 720, 680, 620, and 540  $\mu$ s, previously assigned<sup>41</sup> as the  $-5$  dimer,  $-10$  tetramer,  $-15$  hexamer, and  $-30$  dodecamer, respectively. Dodecamers, potentially associated with memory impairment in mice,<sup>41,44</sup> may be of particular interest to AD pathology. The ATD of  $-5/2$  peak for **ML**-treated **A $\beta$ 42** displayed three features that were assigned to the  $-5$  dimer,  $-10$  tetramer, and  $-15$  hexamer based on their cross section measurements (Figure 3i). Notably, the feature representing **A $\beta$ 42** dodecamer was not observed in the presence of **ML**. The intensity of the  $-15$  hexamer feature is lower compared to that of the **A $\beta$ 42** sample without **ML** (Figure 3h and i). These results indicate that the formation of hexamer and dodecamer is partially and completely inhibited, respectively, by **ML** in solution. In the presence of **ML**, the largest **A $\beta$**  species detected are hexamers because no peaks arrive at shorter arrival times (**A $\beta$ 40** system was also studied; results given in Supporting Information Figure S1).

The ability of **ML** to disaggregate preformed **A $\beta$ 42** aggregates was also explored. The ATD for pure **A $\beta$ 42** incubated on ice for ca. 4 h showed four features corresponding to **A $\beta$ 42** dimers, tetramers, hexamers, and dodecamers (Figure 3j). Concentrated **ML** was added to the **A $\beta$ 42** sample to prepare a 1:5 mixture of **A $\beta$ 42** and **ML**. The  $-5/2$  ATD of the mixture (Figure 3k) exhibited three features corresponding to **A $\beta$ 42** dimers, tetramers, and hexamers. The dodecamers disappeared after the addition of **ML**, which presents that the compound disaggregates preformed dodecamers in solution. Taken together, these IM–MS studies indicate that **ML** not only inhibits dodecamer formation but also disaggregates preformed dodecamers in the early oligomerization of **A $\beta$**  in solution under the MS conditions. **ML** likely continues to interact with a fraction of the smaller oligomers, possibly redirecting them into conformations of lower toxicity (vide infra).

**Control of Metal-Free and Metal-Induced **A $\beta$**  Aggregation by **ML**.** In addition to IM–MS, **ML**'s ability to inhibit the formation of **A $\beta$**  aggregates was evaluated in the absence and presence of metal ions by gel electrophoresis/Western blot (to visualize the size distribution of **A $\beta$**  species) and transmission electron microscopy (TEM) (to examine the morphological change of **A $\beta$**  species) (Figure 4).<sup>21–28</sup> As shown in Figure 4b, the smeared band from **ML**-treated metal-free **A $\beta$ 40**/**A $\beta$ 42** samples (lane 3 in all gels) was indicated and compared to lanes from samples of **A $\beta$**  only or **1**-added **A $\beta$**  (lanes 1 and 2 in all gels). This smeared band is composed of a distribution of **A $\beta$**  species having various molecular weight (MW) and demonstrates that **ML** could direct the production of **A $\beta$**  species with a wide range of MW. **ML** also exhibited noticeable effects on the modulation of metal-induced **A $\beta$**  aggregation. **A $\beta$**  species with a diverse MW distribution (smearing) were presented for samples of **ML**-incubated Cu(II)–**A $\beta$**  or Zn(II)–**A $\beta$**  species (lane 6 in all gels) over compound-free or **1**-treated analogues (lanes 4 and 5 in all gels).<sup>45</sup> **A $\beta$**  aggregates were shorter in **ML**-treated metal-free **A $\beta$**  samples than in nontreated samples as observed by TEM; upon incubation of **ML** with metal–**A $\beta$**  species, unstructured **A $\beta$**  aggregates were mainly visible (Figure 4c).

Furthermore, to understand the structural aspect of **ML**'s control on **A $\beta$**  aggregation (Figure 4), the inhibition experiment was performed employing individual structural components of **ML**, 4-(dimethylamino)phenol (**DAP**), and **1**. As depicted in Supporting Information Figure S10, the effect of **ML** on metal-free and Cu(II)-induced **A $\beta$**  aggregation was more noticeable overall than that of individual structural moieties, **DAP** and **1** (which were relatively less reactive than **ML** with a different MW distribution of resulting **A $\beta$**  species or showed no significant reactivity). In addition, reactivity of a mixture of **DAP** and **1** (**DAP** + **1**) with metal-free **A $\beta$**  and Cu(II)–**A $\beta$**  was indicated to be similar to **DAP** only and relatively less reactive than **ML** showing distinct-sized **A $\beta$**  species. With Zn(II) present, **DAP** and the mixture (**DAP** + **1**) influenced Zn(II)-triggered **A $\beta$**  aggregation, similar to **ML** (Supporting Information Figure S10). Thus, the **DAP** moiety, the structural portion of **ML** that contains the dimethylamino functionality believed to be important for **A $\beta$**  interaction,<sup>21–26,29</sup> could interact and react with metal-free and metal-associated **A $\beta$**  species either less than **ML** (presenting different-sized **A $\beta$** ) or similar to **ML**. Therefore, the reactivity of **ML** with **A $\beta$**  species is proposed to derive mainly from its overall framework rather than from individual structural moieties.

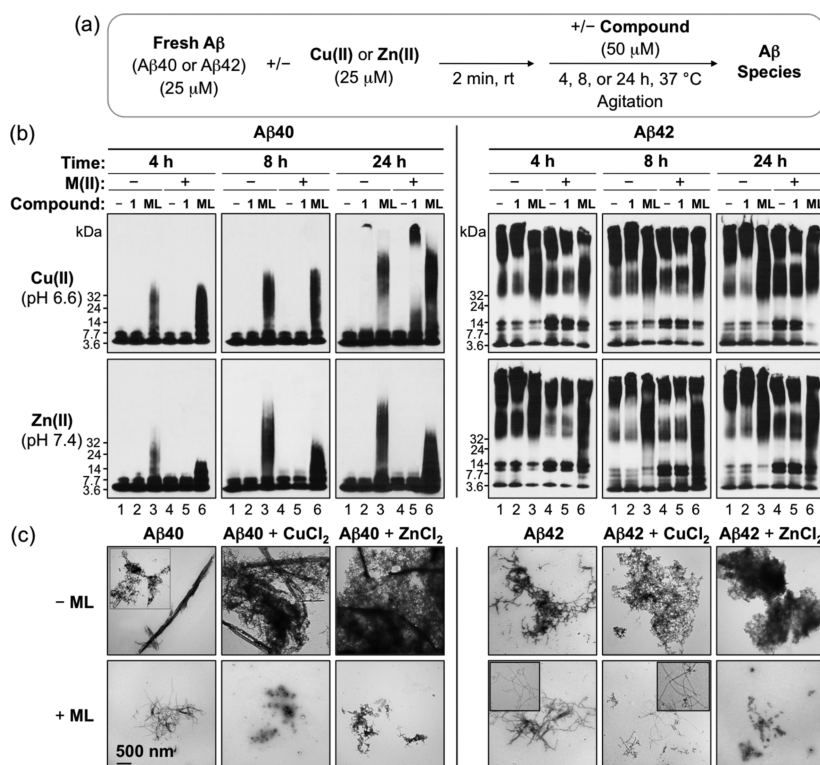


**Figure 4.** Influence of ML or 1 on the formation of metal-free and metal-induced Aβ40/42 aggregates. (a) Scheme of the inhibition experiment. (b) Aβ species were visualized by gel electrophoresis using immunoblotting with an anti-Aβ antibody (6E10). Experimental conditions: Aβ (25 μM); CuCl<sub>2</sub> or ZnCl<sub>2</sub> (25 μM); ML or 1 (50 μM); 4, 8, or 24 h; pH 6.6 (for metal-free and Cu(II) experiments) or 7.4 (for metal-free and Zn(II) experiments); 37 °C; constant agitation. Lanes: (1) Aβ; (2) Aβ + 1; (3) Aβ + ML; (4) Aβ + [CuCl<sub>2</sub> or ZnCl<sub>2</sub>]; (5) Aβ + [CuCl<sub>2</sub> or ZnCl<sub>2</sub>] + 1; (6) Aβ + [CuCl<sub>2</sub> or ZnCl<sub>2</sub>] + ML. (c) TEM images of the 24 h incubated samples from (b).

We further investigated ML's impact on the disaggregation of preformed aggregates of Aβ and metal-Aβ (Supporting Information Figure S11). The MW distributions for both Aβ40 and Aβ42 aggregates, with and without metal ions upon incubation with ML (Supporting Information Figure S11b, lanes 3 and 6) were broadly similar to those in the inhibition experiments (Figure 4b). Metal-free and metal-treated Aβ aggregates with and without 1 presented no discernible difference. TEM revealed that ML could transform preformed aggregates into relatively smaller, amorphous conformations that were more apparent for the Zn(II)-Aβ aggregates relative to the Cu(II)-Aβ aggregates (Supporting Information Figure S11c). Taken together, our inhibition and disaggregation results demonstrate that ML modulates metal-free and metal-induced Aβ aggregation to different extents. This modulatory activity of ML on Aβ aggregation may occur via direct interaction with metal-free or metal-bound Aβ species to form complexes, chelation of metal ions from metal-bound Aβ species, or both, as supported by MS/IM-MS and NMR results (vide supra).

**Regulation of Metal-Free and Metal-Associated Aβ-Induced Toxicity by ML in Living Cells.** We examined the neuroprotective properties of ML toward Aβ- or metal-Aβ-induced toxicity in murine Neuro-2a neuroblastoma cells with and without overexpression of the Swedish mutant human APP (N2aAPP<sup>swe</sup> AD cell line;<sup>46</sup> both Aβ40 and Aβ42 were employed). Cells incubated with Aβ (10 μM) for 24 h in the absence and presence of metal ions (Cu(II) or Zn(II), 10 μM) showed viability of ca. 70% (Aβ), ca. 60–70% (Aβ with Cu(II)), or ca. 70% (Aβ with Zn(II)) (Figure 5a and Supporting Information Figure S12). Upon addition of ML (10 μM) to Aβ-treated N2aAPP<sup>swe</sup> or N2a cells, ca. 90–100% cell survival

was observed with and without metal ions (Figure 5a and Supporting Information Figure S12).<sup>47</sup> Compound 1, compared to ML, was not shown to improve cell viability significantly in N2a cells incubated by both metal-free Aβ and metal-Aβ (Supporting Information Figure S12). Overall, our cell studies suggest that ML may regulate Aβ/metal-Aβ-induced toxicity in living cells.

**ROS Formation Control, Antioxidant Capacity, and BBB Permeability of ML.** From a biological perspective, inhibiting ROS formation by binding and constraining Cu(II) from redox cycling is an attractive feature. Accordingly, we explored the inhibitory ability of ML toward ROS production by the 2-deoxyribose assay.<sup>48</sup> As shown in Figure 5b, copper-mediated generation of hydroxyl radicals was significantly reduced upon treatment with ML, in the absence and presence of Aβ (both freshly prepared and aggregated Aβ species). In addition, ML, compared to its individual structural components, DAP and 1, and the mixture (DAP + 1), inhibited the production of hydroxyl radicals by ca. 2- to 4-fold (Supporting Information Figure S13). This result suggests that the overall structure of ML, particularly its metal binding site that is not preferable for redox cycling of Cu(I/II) (Figure 1),<sup>30</sup> guides its capability of controlling Cu-triggered formation of hydroxyl radicals.

The antioxidant activity of ML was also evaluated by the Trolox equivalent antioxidant capacity (TEAC) assay which measures a compound's ability to quench ABTS cation radicals (ABTS<sup>•+</sup>; ABTS = 2,2'-azino-bis(3-ethylbenzothiazoline-6-sulfonic acid)) in solution<sup>49,50</sup> and in cell lysates. As depicted in Figure 5c, ML scavenged free radicals more effectively in solution than DAP, 1, and Trolox (vitamin E analogue) by a

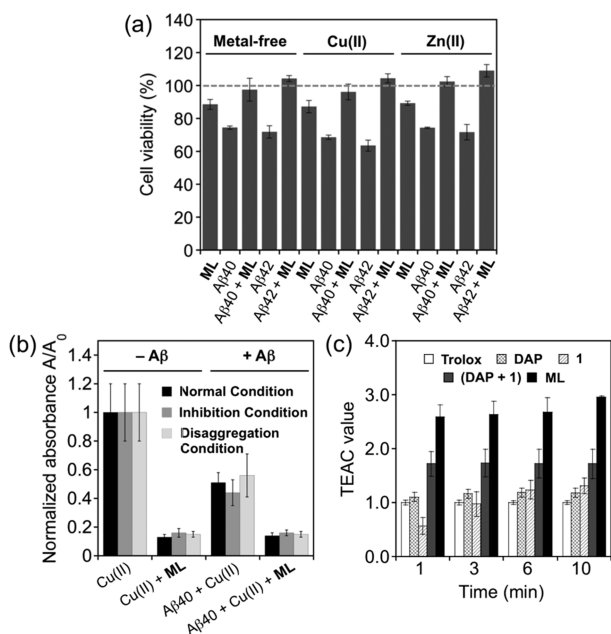


**Figure 5.** Biological activities of ML. (a) Effect of ML on toxicity triggered by metal-free  $A\beta$  and metal- $A\beta$  species in N2aAPP<sup>swe</sup> cells. Cells treated with  $A\beta$ 40/42 (10  $\mu$ M), a metal chloride salt (CuCl<sub>2</sub> or ZnCl<sub>2</sub>; 10  $\mu$ M), or ML (10  $\mu$ M) were incubated for 24 h at 37 °C. Cell viability (%) was determined by the MTT assay compared to cells treated with DMSO only (0–1%, v/v) (MTT = 3-(4,5-dimethyl-2-thiazolyl)-2,5-diphenyl-2H-tetrazolium bromide). Data are mean  $\pm$  SEM,  $P < 0.05$ ,  $n = 3$ . (b) Inhibitory activity toward ROS formation in the absence and presence of freshly prepared  $A\beta$ 40 (normal condition) and  $A\beta$ 40 aggregates (inhibition and disaggregation conditions), determined by the 2-deoxyribose assay. The absorbance values are normalized compared to ligand-free condition ( $A\beta$ /CuCl<sub>2</sub>/ML = 25/10/125  $\mu$ M). (c) Antioxidant activity of ML, DAP, 1, and a mixture of DAP and 1 (DAP + 1) identified by the TEAC assay. The TEAC values are relative to a vitamin E analogue, Trolox (6-hydroxy-2,5,7,8-tetramethylchroman-2-carboxylic acid).

factor of ca. 2.6. Additionally, the mixture (DAP + 1) was observed to scavenge free radicals better than the individual structural component, DAP or 1, but less than ML. The antioxidant capacity of ML was relatively greater than 1 and Trolox within M17 human neuroblastoma cell lysates ( $1.41 \pm 0.15$  for ML;  $0.86 \pm 0.10$  for 1;  $1.00 \pm 0.08$  for Trolox). Overall, the studies of ML's antioxidant activity demonstrate that the presence of both phenolic and quinoline groups within one framework could enhance antioxidant capability.

Lastly, for potential brain applications, the BBB permeability of ML, predicted by Lipinski's rules and logBB (Table 1), was first examined by the Parallel Artificial Membrane Permeability Assay adapted for BBB (PAMPA-BBB).<sup>22,25,26,34,35,51</sup> These values (Table 1), when compared to previously reported BBB permeable molecules,<sup>22,25,26,34,35,51</sup> indicate that ML may cross the BBB. The brain uptake of ML was further investigated using male CD1 mice. The brain and plasma concentrations of ML at 5 min<sup>52</sup> after its administration to mice (10 mg/kg,  $n = 3$ ) by oral gavage were  $14.3 \pm 4.0$  ng/g and  $5.91 \pm 1.24$  ng/mL, respectively. The brain-to-plasma ratio of ML was approximately 2.4. These overall in vivo results in conjunction with the in vitro data (Table 1) suggest that ML is able to cross the BBB and to become available within the CNS. Taken together, other biological properties of ML (e.g., ROS clearance, ROS formation control, BBB permeability) demonstrate this

structural framework could be valuable for potential biological applications (particularly, in the brain).

## CONCLUSIONS

The complexity of AD is suggested to arise from multiple pathological factors, such as  $A\beta$ , metal- $A\beta$ , metal ions, and free radicals; however, the roles of individual elements and, more importantly, their interconnection in disease development remain unclear. To advance our understanding of this aspect and target and control all these features, we have rationally designed a novel molecule, ML, by incorporating structural moieties for  $A\beta$ /metal- $A\beta$  interactions, metal chelation, ROS generation control, and antioxidant activity into a single framework. Water solubility and BBB permeability were considered for potential biological applications, particularly in the brain, as part of our design approach. To the best of our knowledge, ML is the first example of a single designed molecule that can control multiple reactivities, including metal-free and metal-induced  $A\beta$  aggregation, toxicity induced by  $A\beta$  and metal- $A\beta$ , ROS generation, and free radical reactions. ML's properties validate our rational structure-based design strategy and supports the idea that a molecule can be tailored to a specific purpose despite the challenges and complexity of the pathological features of the disease it is intended to examine. There is great heterogeneity in the toxicity landscape of AD.<sup>13</sup> We demonstrated ML's ability to interact with a broad spectrum of  $A\beta$  species (i.e., soluble monomers and oligomers, insoluble fibers). Derivatization of ML to a more lipophilic form may further extend its use to interact and react with membrane-bound  $A\beta$  or  $A\beta$  oligomer channels within membranes. In our future efforts, we intend to extend this work and build a foundation toward the development of chemical tools for uncovering complex AD pathogenesis that will form the basis for the discovery of effective therapeutics for this disease.

## EXPERIMENTAL SECTION

**Materials and Methods.** All reagents were purchased from commercial suppliers and used as received unless otherwise noted.  $A\beta$ 40 and  $A\beta$ 42 were purchased from Anaspec ( $A\beta$ 42 = DAEFRH-DSGYEVHHQKLVFFAEDVGSNKGAIIGLMVGGVVIA; Fremont, CA, U. S. A.). The compound DAP was obtained from Ark Pharm, Inc. (Libertyville, IL, U. S. A.). The compounds 1<sup>30,53</sup> and 5-(dimethylamino)-2-hydroxybenzaldehyde<sup>54</sup> were prepared following previously reported procedures. NMR and mass spectrometric analyses of small molecules were conducted on a 400 MHz Varian NMR spectrometer and a Micromass LCT Electrospray Time-of-Flight (TOF) mass spectrometer, respectively. Trace metal contamination was removed from buffers and solutions used for metal binding and  $A\beta$  experiments (vide infra) by treating with Chelex overnight (Sigma-Aldrich, St. Louis, MO, U. S. A.). Optical spectra were recorded on an Agilent 8453 UV–visible (UV–vis) spectrophotometer. Transmission electron microscopic (TEM) images were taken using a Philips CM-100 transmission electron microscope (Microscopy and Image Analysis Laboratory, University of Michigan, Ann Arbor, MI, U. S. A.). Absorbance values for biological assays, including cell viability assay, PAMPA-BBB, 2-deoxyribose assay, and TEAC assay, were measured on a SpectraMax M5 microplate reader (Molecular Devices, Sunnyvale, CA, U. S. A.). Mass spectra for investigating the interaction of  $A\beta$  with ML in the absence and presence of Cu(II) and Zn(II) were acquired on a traveling-wave Quadrupole TOF (Q-TOF) mass spectrometer (Waters Synapt Prototype, Milford, MA, U. S. A.)<sup>55</sup> and a home-built electrospray ionization (ESI) ion mobility–mass spectrometer.<sup>56</sup> NMR studies of  $A\beta$  with ML or Zn(II) were carried out on a 900 MHz Bruker

spectrometer equipped with a cryogenic probe at Michigan State University in Lansing, MI, U. S. A.

**Synthesis of 4-(Dimethylamino)-2-(((2-(hydroxymethyl)quinolin-8-yl)amino)methyl)phenol (ML).** A solution (dry ethyl acetate (EtOAc), 8.0 mL) of  $1^{30,53}$  (174 mg, 0.99 mmol) and 5-(dimethylamino)-2-hydroxybenzaldehyde<sup>54</sup> (164 mg, 0.99 mmol) was stirred overnight at room temperature. After removing the solvent, the resulting solid material was dissolved in dichloroethane (DCE, 8.0 mL) followed by addition of sodium triacetoxymethylborohydride (NaB(OAc)<sub>3</sub>H, 420 mg, 2.0 mmol). After stirring for 24 h at room temperature, the crude product was purified by column chromatography (SiO<sub>2</sub>, 1:5 hexanes/EtOAc,  $R_f$  = 0.47). The final product (orange powder, HCl salt form) was obtained by recrystallization (upon addition of 1:1 HCl/H<sub>2</sub>O to a MeOH solution of crude products) (198 mg, 0.50 mmol, 51%). <sup>1</sup>H NMR (400 MHz, CD<sub>3</sub>OD,  $\delta$  (ppm)): 8.73 (1H, d,  $J$  = 8.4 Hz), 7.92 (1H, d,  $J$  = 8.8 Hz), 7.80 (1H, d,  $J$  = 8.0 Hz), 7.67 (1H, t,  $J$  = 8.0 Hz), 7.61 (1H, d,  $J$  = 2.8 Hz), 7.55 (2H, m), 7.03 (1H, d,  $J$  = 8.8 Hz), 5.12 (2H, s), 4.74 (2H, s), 3.16 (6H, s). <sup>13</sup>C NMR (100 MHz, DMSO-*d*<sub>6</sub>,  $\delta$  (ppm)): 159.2, 156.0, 141.8, 139.8, 134.5, 133.7, 127.9, 127.8, 126.2, 121.4, 120.7, 119.6, 115.8, 115.1, 106.2, 63.2, 46.0, 42.2. HRMS: [M + H]<sup>+</sup> calcd, 324.1707; found, 324.1697. Anal. Calcd for C<sub>19</sub>H<sub>23</sub>Cl<sub>2</sub>N<sub>3</sub>O<sub>2</sub> (ML·2HCl·H<sub>2</sub>O): C, 55.08; H, 6.08; N, 10.14. Found: C, 54.68; H, 5.96; N, 9.80.

**Ion Mobility–Mass Spectrometry (IM–MS).** Lyophilized A $\beta$ 40 and A $\beta$ 42 were dissolved in 10 mM ammonium acetate buffer (pH 7.4) to generate a final peptide concentration of 10  $\mu$ M for all mass spectrometry experiments. Mass spectra were recorded on a prototype of the commercial Waters Synapt instrument (Milford, MA, U. S. A.)<sup>55</sup> and a home-built ESI ion mobility–mass spectrometer.<sup>56</sup> Briefly, for ion mobility measurements, ions were generated continuously by a nano-ESI source, focused, and stored in the ion funnel. The ions were then pulsed into a temperature-controlled drift cell filled with 3–5 torr helium gas, where they gently pass through under the influence of a weak electric field. The ions exiting the drift cell were mass analyzed with a quadrupole mass filter, detected by a conversion dynode and channel electron multiplier, and recorded as a function of time to obtain the arrival time distributions (ATDs).

The velocity of the ions in the drift cell  $v_d$  is proportional to the electric field  $E$

$$v_d = KE \quad (1)$$

Here, the proportionality constant  $K$  is termed ion mobility. The absolute ion mobility is dependent on the temperature ( $T$ ) and the pressure ( $P$ ) of the buffer gas (He), so it is typically converted to the reduced mobility  $K_0$

$$K_0 = K \cdot \frac{P}{760} \cdot \frac{273.16}{T} \quad (2)$$

The ions exiting the drift cell are mass analyzed and detected as a function of the arrival time,  $t_A$ . The reduced mobility  $K_0$  can be determined from the instrument parameters by using eq 3 and plotting  $t_A$  versus  $P/V$ <sup>57</sup>

$$t_A = \frac{l^2}{K_0} \cdot \frac{273.16}{760T} \cdot \frac{P}{V} + t_0 \quad (3)$$

In eq 3,  $l$  is the length of the drift cell (4.503 cm),  $V$  is the voltage across the drift cell, and  $t_0$  is the time the ions spend outside the drift cell before hitting the detector. All of these quantities are either known constants or are measured for each experiment.

The reduced ion mobility  $K_0$  can be related to the collision cross section  $\Omega$  using kinetic theory<sup>58</sup>

$$K_0 = \frac{3q}{16N} \left( \frac{2\pi}{\mu k_B T} \right)^{1/2} \frac{1}{\Omega} \quad (4)$$

Here,  $q$  is the ion charge,  $N$  is the buffer gas number density at STP,  $\mu$  is the reduced mass of the ion–He collision, and  $k_B$  is the Boltzmann constant. The measured reduced mobility ( $K_0$ ) and the collision cross

section ( $\Omega$ ) provide information about the three-dimensional configurations of the ions. For peptide and protein ions, the secondary/tertiary structural information and the oligomerization states can be identified by comparison with modeling.<sup>41</sup>

**2D NMR Spectroscopy.** The interaction of prefibrillar A $\beta$ 40 with ML was determined by a series of 2D band-Selective Optimized Flip-Angle Short Transient Heteronuclear Multiple Quantum Correlation (SOFAS-TMQC) experiments by titrating a 80  $\mu$ M solution of A $\beta$ 40 with a 40 mM stock solution of ML in DMSO.<sup>59</sup> The influence of DMSO on the spectrum of A $\beta$ 40 is minor at the maximum concentration of DMSO used (1% v/v final concentration).<sup>23</sup> NMR samples were prepared from <sup>15</sup>N-labeled A $\beta$ 40 (rPeptide, Bogart, GA, U. S. A.) by first dissolving the peptide in 1% NH<sub>4</sub>OH, lyophilizing, and then resuspending in 150  $\mu$ L of 1 M NaOD (pH 10). The peptide was then diluted 1:1 with deuterated Tris–DCl for a final buffer concentration of 50 mM Tris–DCl, verified to be pD 7.3 before the start of each titration using the relation pD = pH meter reading + 0.4.<sup>60</sup> Trace metals were removed by treating all buffers and solutions with Chelex (Sigma-Aldrich, St. Louis, MO, U. S. A.) prior to the experiment. Each spectrum was obtained from 256  $t_1$  experiments, 16 transients, and a 100 ms recycle delay on a Bruker Avance 900 MHz spectrometer at 4 °C. 2D data were processed using TOPSPIN 2.1 (from Bruker). Resonance assignment and volume fit calculations were performed with SPARKY 3.113 using published assignments for A $\beta$ 40 as a guide.<sup>36,61,62</sup>

**Saturation Transfer Difference (STD) NMR Spectroscopy.** For the STD NMR experiments, an 80  $\mu$ M solution of fibrillar A $\beta$ 40 was prepared by incubating for 24 h at 37 °C with constant agitation in 50 mM deuterated Tris–DCl, 95% D<sub>2</sub>O with or without 80  $\mu$ M ZnCl<sub>2</sub> at pD 7.4 (corrected for the isotope effect). To minimize the aggregation of ML that occurs at high concentration at neutral pH, ML was added to fibrillar A $\beta$ 40 by dilution from a 3.1 mM stock solution in acidic 1 mM DCl (pD 4) for a final ML:A $\beta$ 40 molar ratio of 10:1 (200  $\mu$ M ML:20  $\mu$ M A $\beta$ 40) in 50 mM deuterated Tris–DCl, 95% D<sub>2</sub>O with or without 80  $\mu$ M ZnCl<sub>2</sub> at pD 7.4. STD experiments were acquired with a train of 60 dB Gaussian-shaped pulses of 50 ms duration at centered at either –2.0 ppm (on resonance<sup>63–65</sup>) or 100 ppm (off resonance) with a total saturation time of 3 s on a Bruker 500 MHz (metal-free samples) or 900 MHz spectrometer (Zn(II) samples).<sup>66</sup> A total of 2048 transients with a 2 s recycle delay were collected for all spectra. Chemical shifts are referenced to water due to the potential interaction of A $\beta$ 40 with the chemical shift standard sodium 4,4-dimethyl-4-silapentane-1-sulfonate (DSS).<sup>67</sup>

**Docking of ML with Fibrillar A $\beta$ 40.** Flexible ligand docking studies of ML against the A $\beta$ 40 fiber were conducted using AutoDock4.2.<sup>68</sup> The starting conformations of the fiber were obtained from previous solid-state NMR models of A $\beta$ 40 fibers (PDB LMO and LMN); current structural constraints are consistent with both models for A $\beta$ 40 fibers formed under agitation.<sup>69</sup> A model for ML was first constructed and energy minimized using the PRODRG server.<sup>70</sup> Prior to docking, hydrogen atoms were added to ML and the A $\beta$ 40 fiber using AutoDock Tools.<sup>68</sup> Kollman charges<sup>71</sup> were used for the A $\beta$ 40 fiber and Gasteiger charges<sup>72,73</sup> were introduced to ML. An electrostatics grid map of the system and atomic affinity grid maps for each atom type were then set up using AutoGrid 4.2, using 126 points in each dimension centered on the A $\beta$ 40 fiber with a grid spacing of 0.636 Å.<sup>74</sup> Docking was performed using a Lamarckian Genetic Algorithm to search the conformation space of ML for low energy binding orientations.<sup>74</sup> An initial random population of 200 individuals was used to start the docking run, which was set to have a maximum of 25  $\times$  10<sup>6</sup> energy evaluations and a maximum of 270 000 generations. The resulting structures from docking were clustered using an RMSD cutoff of 2.0 Å.

**Metal Binding Experiments.** Unless otherwise stated, metal binding properties of ML (50  $\mu$ M, 1% v/v DMSO) and **1** (50 or 500  $\mu$ M, 1% DMSO) were investigated in a Chelex-treated buffered solution containing 20 mM 2-[4-(2-hydroxyethyl)piperazin-1-yl]ethanesulfonic acid (HEPES), pH 7.4, and 150 mM NaCl. To a solution of ML or **1**, 1 equiv of CuCl<sub>2</sub> or ZnCl<sub>2</sub> was treated and incubated for 30 min (for ML with CuCl<sub>2</sub>), 1 h (for ML with ZnCl<sub>2</sub>),



or 10 min (for **1** with  $\text{CuCl}_2$  or  $\text{ZnCl}_2$ ) at room temperature. To examine the metal selectivity of **ML** or **1**, 1 or 20 equiv of  $\text{MgCl}_2$ ,  $\text{CaCl}_2$ ,  $\text{MnCl}_2$ ,  $\text{FeCl}_2$ ,  $\text{CoCl}_2$ ,  $\text{NiCl}_2$ , and  $\text{ZnCl}_2$  (for  $\text{Cu(II)}$  selectivity) or  $\text{CuCl}_2$  (for  $\text{Zn(II)}$  selectivity) was first treated to a solution containing 50  $\mu\text{M}$  of ligand (**ML** or **1**). The spectra were recorded after an additional 5 min incubation at room temperature. The  $\text{Fe(II)}$  samples were maintained anaerobically by purging the solutions with  $\text{N}_2$ .  $\text{CuCl}_2$  (for  $\text{Cu(II)}$  selectivity experiments) or  $\text{ZnCl}_2$  (for  $\text{Zn(II)}$  selectivity experiments) (50  $\mu\text{M}$ ) was then added to a solution of compound (**ML** or **1**) and a divalent metal chloride salt. The spectra were taken after an additional 5 min incubation at room temperature. Quantification of metal selectivity was calculated by comparing and normalizing the absorption values of metal–ligand complexes at 485 nm ( $\text{Cu(II)}$  selectivity of **ML**), 291 nm ( $\text{Cu(II)}$  selectivity of **1**), and 425 nm ( $\text{Zn(II)}$  selectivity of **ML**) to the absorption at this wavelength before and after the addition of  $\text{CuCl}_2$  ( $A_M/A_{\text{Cu}}$ ) or  $\text{ZnCl}_2$  ( $A_M/A_{\text{Zn}}$ ).

**Solution Speciation Studies for **ML**, **1**,  $\text{Cu(II)}$ –**ML/1**, and  $\text{Zn(II)}$ –**ML/1** Complexes.** The  $pK_a$  values for **ML** and **1** were determined by UV–vis variable-pH titrations based on a previously reported procedure.<sup>22–26</sup> To obtain  $pK_a$  values for the ligands, a solution (100 mM NaCl, 10 mM NaOH, pH 12) of **ML** or **1** (50  $\mu\text{M}$ ) was titrated with small aliquots of HCl to obtain at least 30 spectra in the range of pH 2–8 (for **ML**) or pH 2–9 (for **1**). In addition, to investigate  $\text{Cu(II)}$  or  $\text{Zn(II)}$  binding to ligand at various pHs, solutions containing a ligand (**ML** or **1**) and a metal chloride salt ( $[\text{M(II)}]:[\text{L}] = 1:2$ ;  $[\text{CuCl}_2] = 25 \mu\text{M}$ ;  $[\text{ZnCl}_2] = 50 \mu\text{M}$  (for **ML**) or 250  $\mu\text{M}$  (for **1**)) were prepared. The solution was titrated with small aliquots of HCl. At least 30 spectra were measured over the range of pH 2–9 for both  $\text{Cu(II)}$  and  $\text{Zn(II)}$  systems. The acidity and stability constants were calculated by using the HypSpec program (Protonic Software, Leeds, UK).<sup>75</sup> Speciation diagrams of ligands and their corresponding metal complexes were modeled using the HySS2009 program (Protonic Software, Leeds, UK).<sup>76</sup>

**$A\beta$  Aggregation Experiments.**  $A\beta$  experiments were performed according to previously published methods.<sup>21–28,77</sup> Prior to experiments,  $A\beta 40$  or  $A\beta 42$  was dissolved in ammonium hydroxide ( $\text{NH}_4\text{OH}$ , 1% v/v, aq), aliquoted, lyophilized overnight, and stored at  $-80^\circ\text{C}$ . For experiments described herein, a stock solution of  $A\beta$  was prepared by dissolving lyophilized peptide in 1%  $\text{NH}_4\text{OH}$  (10  $\mu\text{L}$ ) and diluting with  $\text{ddH}_2\text{O}$ . The concentration of the solution was determined by measuring the absorbance of the solution at 280 nm ( $\epsilon = 1450 \text{ M}^{-1}\text{cm}^{-1}$  for  $A\beta 40$ ;  $\epsilon = 1490 \text{ M}^{-1}\text{cm}^{-1}$  for  $A\beta 42$ ). The peptide stock solution was diluted to a final concentration of 25  $\mu\text{M}$  in Chelex-treated buffered solution containing HEPES (20  $\mu\text{M}$ , pH 6.6 for metal-free and  $\text{Cu(II)}$  samples; pH 7.4 for metal-free and  $\text{Zn(II)}$  samples) and NaCl (150  $\mu\text{M}$ ). For the inhibition studies,<sup>21–28,77</sup> a compound (final concentration 50  $\mu\text{M}$ , 1% v/v DMSO) was added to the sample of  $A\beta$  (25  $\mu\text{M}$ ) in the absence and presence of a metal chloride salt ( $\text{CuCl}_2$  or  $\text{ZnCl}_2$ , 25  $\mu\text{M}$ ) followed by incubation at  $37^\circ\text{C}$  with constant agitation for 4, 8, and 24 h. For the disaggregation studies,<sup>21–28,77</sup>  $A\beta$  with and without metal ions was incubated for 24 h at  $37^\circ\text{C}$  with constant agitation prior to treatment with a compound (50  $\mu\text{M}$ ). The resulting samples containing  $A\beta$ , a metal chloride salt, and a compound were incubated at  $37^\circ\text{C}$  with constant agitation for 4, 8, and 24 h.

**Gel Electrophoresis.** Samples from the inhibition and disaggregation experiments were analyzed by gel electrophoresis with Western blot using anti- $A\beta$  antibody (6E10).<sup>21–28,77</sup> Each sample (10  $\mu\text{L}$ ) was separated on a 10–20% Tris–tricine gel (Invitrogen, Grand Island, NY, U. S. A.). Following separation, the proteins were transferred onto nitrocellulose which was blocked with bovine serum albumin (BSA, 3% w/v, Sigma-Aldrich, St. Louis, MO, U. S. A.) in Tris-buffered saline (TBS) containing 0.1% Tween-20 (TBS-T) for 2 or 3 h at room temperature. The membranes were incubated with antibody (6E10, 1:2000, Covance, Princeton, NJ, U. S. A.) in a solution of 2% BSA (w/v in TBS-T) overnight at  $4^\circ\text{C}$ . After washing, the horseradish peroxidase-conjugated goat antimouse secondary antibody (1:5000) in 2% BSA was added for 1 h at room temperature. The ThermoScientific SuperSignal West Pico Chemiluminescent

Substrate (Thermo Scientific, Rockford, IL, U. S. A.) was used to visualize protein bands.

**Transmission Electron Microscopy (TEM).** Samples for TEM were prepared according to previously reported methods.<sup>21–28,77</sup> Glow-discharged grids (Formar/Carbon 300-mesh, Electron Microscopy Sciences, Hatfield, PA, U. S. A.) were treated with  $A\beta$  samples from the inhibition and disaggregation experiments (5  $\mu\text{L}$ ) for 2 min at room temperature. Excess sample was removed using filter paper followed by washing twice with  $\text{ddH}_2\text{O}$ . Each grid was incubated with uranyl acetate (1% w/v  $\text{ddH}_2\text{O}$ , 5  $\mu\text{L}$ , 1 min). Upon removal of excess uranyl acetate, the grids were dried for 15 min at room temperature. Images from each sample were taken on a Philips CM-100 transmission electron microscope (80 kV, 25 000 $\times$  magnification).

**Cell Viability Measurements.** The N2a cell line was purchased from the American Type Cell Collection (ATCC, Manassas, VA, U. S. A.). N2a cells stably overexpressing the Swedish mutant (K670N and M671L) human APP (N2aAPPswe)<sup>46</sup> were the generous gift of Professor Gopal Thinakaran (University of Chicago). Both cell lines were maintained in media containing 45% DMEM, 50% OPTI-MEM, 5% fetal bovine serum (FBS, Atlanta Biologicals, Lawrenceville, GA, U. S. A.), 100 U/mL penicillin (GIBCO, Grand Island, NY, U. S. A.), and 100 mg/mL streptomycin (GIBCO). For the N2aAPPswe cell line, 0.2 mg/mL G418 (Geneticin, GIBCO) was added to the culture medium. The cells were grown in a humidified atmosphere with 5%  $\text{CO}_2$  at  $37^\circ\text{C}$ . For the MTT assay (MTT = 3-(4,5-dimethyl-2-thiazolyl)-2,5-diphenyl-2H-tetrazolium bromide, Sigma-Aldrich), cells were seeded in a 96 well plate (15 000 cells/100  $\mu\text{L}$ ). The cells were then treated with  $A\beta$  (10  $\mu\text{M}$ ) with or without  $\text{CuCl}_2$  or  $\text{ZnCl}_2$  (10  $\mu\text{M}$ ) followed by the addition of **ML** or **1** (final concentration 10  $\mu\text{M}$ , 1% v/v final DMSO concentration). After 24 h incubation, 25  $\mu\text{L}$  MTT (5 mg/mL in phosphate buffered saline (PBS, pH 7.4, GIBCO) was added to each well and the plate was incubated for 4 h at  $37^\circ\text{C}$ . Formazan produced by the cells was solubilized by addition of an acidic solution of *N,N*-dimethylformamide (50%, v/v, aq) and sodium dodecyl sulfate (SDS, 20%, w/v) overnight at room temperature in the dark. The absorbance was measured at 600 nm using a microplate reader. The concentrations (0 to 10  $\mu\text{M}$ ) of **ML** or **1**, which do not interfere with the analysis of MTT assay, were selected for the cell studies.

**2-Deoxyribose Assay.** The ability of **ML**, **DAP**, **1**, and a mixture of **DAP** and **1** (**DAP** + **1**) to suppress free radical Fenton chemistry was determined by the 2-deoxyribose assay. The assay was performed based on previously established methods with some modifications.<sup>48</sup> Chelexed solutions were used, and reactions (total volume, 200  $\mu\text{L}$ ) were setup by mixing, in the following order, buffer (50 mM  $\text{NaH}_2\text{PO}_4$ , pH 7.2), ligand (125  $\mu\text{M}$ ),  $\text{CuCl}_2$  (10  $\mu\text{M}$ ), 2-deoxyribose (15 mM),  $\text{H}_2\text{O}_2$  (200  $\mu\text{M}$ ), and sodium ascorbate (2 mM) and allowed to react for 1 h at  $37^\circ\text{C}$  with constant agitation. The reactions were quenched upon addition of trichloroacetic acid (200  $\mu\text{L}$  of 2.8% w/v) and 2-thiobarbituric acid (200  $\mu\text{L}$  of 1% w/v) and heated at  $100^\circ\text{C}$  for 20 min, cooled for 5 min, and their absorbance values at 532 nm measured immediately afterward. In addition, samples without ligand were prepared as a control. Experiments were performed in triplicates. Normalized absorbance values ( $A/A_0$ ) were calculated by taking the absorbance ( $A$ ) and dividing by the absorbance of the control ( $A_0$ ).

Experiments in the presence of  $A\beta$  (25  $\mu\text{M}$ ) were carried out in three formats. (a) Experiments with freshly prepared  $A\beta 40$  were conducted in the “normal condition” as for  $A\beta$ -free samples in which all reagents were added simultaneously, shaken for 2 h at  $37^\circ\text{C}$ , and heated to develop the pink chromogen at 532 nm. (b) Experiments were also performed in the “inhibition condition” in which  $A\beta/\text{CuCl}_2/\text{ML}$  (25/10/125  $\mu\text{M}$ ) samples were mixed and incubated for 24 h, then assay reagents were added (2-deoxyribose,  $\text{H}_2\text{O}_2$ , and ascorbate), and the assay was carried out. (c) Experiments were also completed in the “disaggregation condition” in which **ML** (125  $\mu\text{M}$ ) was added to  $A\beta$  aggregates generated by treating  $A\beta$  (25  $\mu\text{M}$ ) with  $\text{CuCl}_2$  (10  $\mu\text{M}$ ) for 24 h and the resulting solution was incubated for 24 h, at which point the assay was carried out. Copper-only and copper-**ML**-only controls were prepared for comparison. Data was analyzed as for  $A\beta$ -

free experiments, by normalizing the absorbance at 532 nm against copper-only controls.

**Trolox Equivalent Antioxidant Capacity (TEAC) Assay.** The antioxidant activity of **ML** and **1** was determined by the TEAC assay in EtOH and with M17 human neuroblastoma cell lysates. (a) The assay in solution was performed according to a previously reported method with slight modifications.<sup>49,50</sup> To generate blue ABTS cation radicals (ABTS<sup>•+</sup>; ABTS = 2,2'-azino-bis(3-ethylbenzothiazoline-6-sulfonic acid) diammonium salt; Sigma-Aldrich), a solution of ABTS (7.0 mM) and potassium persulfate (2.5 mM; Sigma-Aldrich) was prepared in 5 mL of water and incubated for 16 h at room temperature in the dark. The resulting solution was diluted with EtOH to an absorbance of ca. 0.7 at 734 nm. ABTS<sup>•+</sup> solution (200  $\mu$ L) was added to the wells of a clear 96 well plate and incubated for 5 min at 30 °C. Various final concentrations (0, 1, 2.5, 5, 7.5, 10, and 15  $\mu$ M) of **ML**, **DAP**, **1**, (**DAP** + **1**) or Trolox (Trolox = 6-hydroxy-2,5,7,8-tetramethylchroman-2-carboxylic acid; Sigma-Aldrich; dissolved in EtOH) were added and incubated with the ABTS<sup>•+</sup> solution at 30 °C for different time periods (1, 3, 6, and 10 min). The percent inhibition was calculated according to the measured absorbance at 734 nm (% inhibition =  $100 \times (A_0 - A)/A_0$ ) and was plotted as a function of ligand concentration. The TEAC value of compounds for each time point was calculated as a ratio of the slope of the compound to that of Trolox. The measurements were carried out in triplicate. (b) The assay employing cell lysates was conducted following the protocol of the antioxidant assay kit purchased from Cayman Chemical Company (Ann Arbor, MI, U. S. A.), with minor modifications. The human neuroblastoma SK-N-BE(2)-M17 (M17) cells were used for this assay. This cell line purchased from ATCC (Manassas, VA, U. S. A.) was maintained in media containing 1:1 minimum Essential Media (MEM, GIBCO) and Ham's F12K Kaighn's Modification Media (F12K, GIBCO), 10% (v/v) fetal bovine serum (FBS, GIBCO), 100 U/mL penicillin (GIBCO), and 100 mg/mL streptomycin (GIBCO). The cells were grown and maintained at 37 °C in a humidified atmosphere with 5% CO<sub>2</sub>. For the antioxidant assay using cell lysates, cells were seeded in a 6 well plate and grown to approximately 80–90% confluence. Cell lysates were prepared following a previously reported method with modifications.<sup>78</sup> M17 cells were washed once with cold PBS (pH 7.4, GIBCO) and harvested by gently pipetting off adherent cells with cold PBS. The cell pellet was generated by centrifugation (2000g for 10 min at 4 °C). This cell pellet was sonicated on ice (5 s pulses five times with 20 s intervals between each pulse) in 2 mL of cold Assay Buffer (5 mM potassium phosphate, pH 7.4, containing 0.9% NaCl and 0.1% glucose). The cell lysates were centrifuged at 10 000g for 10 min at 4 °C. The supernatant was removed and stored on ice until use. To standard and sample 96 wells, 10  $\mu$ L of the supernatant of cell lysates was delivered followed by addition of compound, metmyoglobin, ABTS, and H<sub>2</sub>O<sub>2</sub> in order. After 5 min incubation at room temperature on a shaker, absorbance values at 750 nm were recorded. The final concentrations (0.045, 0.090, 0.135, 0.180, 0.225, and 0.330 mM) of **ML**, **1**, and Trolox were used. The percent inhibition was calculated according to the measured absorbance (% inhibition =  $(A_0 - A)/A_0$ , where  $A_0$  is absorbance of the supernatant of cell lysates) and was plotted as a function of compound concentration. The TEAC value of ligands was calculated as a ratio of the slope of the standard curve of the compound to that of Trolox. The measurements were conducted in triplicate.

**Parallel Artificial Membrane Permeability Adapted for the Blood-Brain Barrier (PAMPA-BBB) Assay.** PAMPA-BBB experiments were carried out using the PAMPA Explorer kit (pION Inc., Billerica, MA, U. S. A.) with modification to previously reported protocols.<sup>22,25,26,34,35,51</sup> Each stock solution was diluted with Prisma HT buffer (pH 7.4, pION) to a final concentration of 25  $\mu$ M (1% v/v final DMSO concentration). The resulting solution was added to wells of the donor plate (200  $\mu$ L, number of replicates = 12 (for **ML**) and 11 (for **1**)). BBB-1 lipid formulation (5  $\mu$ L, pION) was used to coat the polyvinylidene fluoride (PVDF, 0.45  $\mu$ M) filter membrane on the acceptor plate. This acceptor plate was placed on top of the donor plate forming a sandwich. Brain sink buffer (BSB, 200  $\mu$ L, pION) was added to each well of the acceptor plate. The sandwich was incubated

for 4 h at ambient temperature without stirring. UV–vis spectra of the solutions in the reference, acceptor, and donor plates were measured using a microplate reader. The PAMPA Explorer software v. 3.5 (pION) was used to calculate  $-\log P_e$  for each compound. CNS+/- designations were assigned by comparison to compounds that were identified in previous reports.<sup>34,35,51</sup>

**Brain Uptake Studies.** The experiments of **ML**'s brain uptake were carried out using male CD1 mice (purchased from Vital River Laboratory Animal Technology Co. Ltd. (Beijing, China)) by Contract Research Organization, Shanghai ChemPartner Co., Ltd. (Shanghai, China). The studies reported here adhere to the principles of the Association for Assessment and Accreditation of Laboratory Animal Care (AAALAC) International. **ML** (10 mg/kg; single dose; sterile water) was administered to mice by oral gavage. At 5 min postdose<sup>52</sup> ( $n = 3$  at each time point), 150  $\mu$ L of blood was withdrawn via retro orbital puncture or cardiac puncture and transferred into tubes with spray-coated K<sub>2</sub>EDTA as anticoagulant. Blood samples were put on ice and centrifuged to obtain plasma samples (2000g, 5 min, 4 °C). Immediately following blood collection, mice were euthanized by pure CO<sub>2</sub> inhalation and the whole brain was collected, rinsed with cold saline, dried on filter paper, and weighed. The brain samples were immediately homogenized with three volumes (v/w) of homogenizing solution (PBS). Both plasma and brain samples were added with an internal standard (propranolol) in acetonitrile (CH<sub>3</sub>CN; protein precipitation). The mixture was vortexed for 2 min and centrifuged at 14 000 rpm for 5 min and an aliquot of the supernatant was analyzed for concentration of **ML** by LC-MS/MS (UPLC/MS-MS API-5500, Framingham, MA, U. S. A.), with analytical lower limit of quantitation (LLOQ) values for **ML** at 1 ng/mL (plasma) and 4 ng/mL (brain). The supernatant was stored at  $-80$  °C prior to analysis.

## ■ ASSOCIATED CONTENT

### ● Supporting Information

Additional mass spectra, UV–vis spectra, docking diagrams, cluster energy analyses, electrophoresis visualizations, TEM images, and selectivity, speciation, and cytotoxicity, and inhibitory activity studies. This material is available free of charge via the Internet at <http://pubs.acs.org>.

## ■ AUTHOR INFORMATION

### Corresponding Authors

A. Ramamoorthy. E-mail: [ramamoor@umich.edu](mailto:ramamoor@umich.edu).

M. T. Bowers. E-mail: [bowers@chem.ucsb.edu](mailto:bowers@chem.ucsb.edu).

M. H. Lim. E-mail: [mhlim@unist.ac.kr](mailto:mhlim@unist.ac.kr).

### Present Address

$\Delta$ SGS Life Science Services, 6490 Vipond Drive, Mississauga, Ontario L5T 1W8, Canada

### Notes

The authors declare no competing financial interest.

## ■ ACKNOWLEDGMENTS

This work was supported by funding from the National Institutes of Health to A.R. (GM084018, GM095640, and RR023597) and to M.T.B. (AG047116), the American Heart Association, Ruth K. Broad Biomedical Foundation, Alfred P. Sloan Fellowship, Rush Alzheimer's Disease Core Center (P30AG010161), and the National Science Foundation (CHE-1253155) (to M.H.L.). This work was also supported by the 2013 Research Fund (Project Number 1.130068.01) of UNIST (Ulsan National Institute of Science and Technology) (to M.H.L.). C.K. thanks the Basic Science Research Program through the National Research Foundation of Korea funded by the Ministry of Education, Science and Technology (2012001725) for support. We are grateful to Professor Gopal Thinakaran (University of Chicago) for the generous

supply of the N2aAPP<sub>swe</sub> cell line. We also thank Alaina DeToma for experimental assistance on the PAMPA assay.

## REFERENCES

- (1) Thies, W.; Bleiler, L.; Alzheimer's Association. *Alzheimer's Dementia* **2013**, *9*, 208–245.
- (2) Corbett, A.; Pickett, J.; Burns, A.; Corcoran, J.; Dunnett, S. B.; Edison, P.; Hagan, J. J.; Holmes, C.; Jones, E.; Katona, C.; Kearns, L.; Kehoe, P.; Mudher, A.; Passmore, A.; Shepherd, N.; Walsh, F.; Ballard, C. *Nat. Rev. Drug Discov.* **2012**, *11*, 833–846.
- (3) Jakob-Roetne, R.; Jacobsen, H. *Angew. Chem. Int. Ed.* **2009**, *48*, 3030–3059.
- (4) Hamley, I. W. *Chem. Rev.* **2012**, *112*, 5147–5192.
- (5) Kepp, K. P. *Chem. Rev.* **2012**, *112*, 5193–5239.
- (6) Savelieff, M. G.; Lee, S.; Liu, Y.; Lim, M. H. *ACS Chem. Biol.* **2013**, *8*, 856–865.
- (7) Duce, J. A.; Bush, A. I. *Prog. Neurobiol.* **2010**, *92*, 1–18.
- (8) DeToma, A. S.; Salamekh, S.; Ramamoorthy, A.; Lim, M. H. *Chem. Soc. Rev.* **2012**, *41*, 608–621.
- (9) Scott, L. E.; Orvig, C. *Chem. Rev.* **2009**, *109*, 4885–4910.
- (10) Que, E. L.; Domaille, D. W.; Chang, C. J. *Chem. Rev.* **2008**, *108*, 1517–1549.
- (11) Zatta, P.; Drago, D.; Bolognin, S.; Sensi, S. L. *Trends Pharmacol. Sci.* **2009**, *30*, 346–355.
- (12) Pithadia, A. S.; Lim, M. H. *Curr. Opin. Chem. Biol.* **2012**, *16*, 67–73.
- (13) Miller, Y.; Ma, B.; Nussinov, R. *Chem. Rev.* **2010**, *110*, 4820–4838.
- (14) Haass, C.; Selkoe, D. J. *Nat. Rev. Mol. Cell Biol.* **2007**, *8*, 101–112.
- (15) Shankar, G. M.; Li, S.; Mehta, T. H.; Garcia-Munoz, A.; Shepardson, N. E.; Smith, I.; Brett, F. M.; Farreel, M. A.; Rowan, M. J.; Lemere, C. A.; Regan, C. M.; Walsh, D. M.; Sabatini, B. L.; Selkoe, D. J. *Nat. Med.* **2008**, *14*, 837–842.
- (16) Faller, P.; Hureau, C. *Dalton Trans.* **2009**, 1080–1094.
- (17) Faller, P. *ChemBioChem* **2009**, *10*, 2837–2845.
- (18) Telpoukhovskaia, M.; Orvig, C. *Chem. Soc. Rev.* **2013**, *42*, 1836–1846.
- (19) Rodríguez-Rodríguez, C.; Telpoukhovskaia, M.; Orvig, C. *Coord. Chem. Rev.* **2012**, *256*, 2308–2332.
- (20) Braymer, J. J.; DeToma, A. S.; Choi, J.-S.; Ko, K. S.; Lim, M. H. *Int. J. Alzheimer's Dis.* **2011**, 2011:623051.
- (21) Hindo, S. S.; Mancino, A. M.; Braymer, J. J.; Liu, Y.; Vivekanandan, S.; Ramamoorthy, A.; Lim, M. H. *J. Am. Chem. Soc.* **2009**, *131*, 16663–16665.
- (22) Choi, J.-S.; Braymer, J. J.; Nanga, R. P. R.; Ramamoorthy, A.; Lim, M. H. *Proc. Natl. Acad. Sci. U. S. A.* **2010**, *107*, 21990–21995.
- (23) Braymer, J. J.; Choi, J.-S.; DeToma, A. S.; Wang, C.; Nam, K.; Kampf, J. W.; Ramamoorthy, A.; Lim, M. H. *Inorg. Chem.* **2011**, *50*, 10724–10734.
- (24) Choi, J.-S.; Braymer, J. J.; Park, S. K.; Mustafa, S.; Chae, J.; Lim, M. H. *Metallomics* **2011**, *3*, 284–291.
- (25) Pithadia, A. S.; Kochi, A.; Soper, M. T.; Beck, M. W.; Liu, Y.; Lee, S.; DeToma, A. S.; Ruotolo, B. T.; Lim, M. H. *Inorg. Chem.* **2012**, *51*, 12959–12967.
- (26) Liu, Y.; Kochi, A.; Pithadia, A. S.; Lee, S.; Nam, Y.; Beck, M. W.; He, X.; Lee, D.; Lim, M. H. *Inorg. Chem.* **2013**, *52*, 8121–8130.
- (27) Hyung, S. J.; DeToma, A. S.; Brender, J. R.; Lee, S.; Vivekanandan, S.; Kochi, A.; Choi, J. S.; Ramamoorthy, A.; Ruotolo, B. T.; Lim, M. H. *Proc. Natl. Acad. Sci. U. S. A.* **2013**, *110*, 3743–3748.
- (28) DeToma, A. S.; Choi, J.-S.; Braymer, J. J.; Lim, M. H. *ChemBioChem* **2011**, *12*, 1198–1201.
- (29) Kung, H. F.; Lee, C.-W.; Zhuang, Z.-P.; Kung, M.-P.; Hou, C.; Plössl, K. J. *Am. Chem. Soc.* **2001**, *123*, 12740–12741.
- (30) Lim, M. H.; Wong, B. A.; Pitcock, W. H.; Mokshagundam, D.; Baik, M.-H.; Lippard, S. J. *J. Am. Chem. Soc.* **2006**, *128*, 14364–14373.
- (31) Orhan Puskullu, M.; Tekiner, B.; Suzen, S. *Mini Rev. Med. Chem.* **2013**, *13*, 365–372.
- (32) Havsteen, B. H. *Pharmacol. Ther.* **2002**, *96*, 67–202.
- (33) Rice-Evans, C. A.; Miller, N. J.; Paganga, G. *Free Radical Biol. Med.* **1996**, *20*, 933–956.
- (34) Di, L.; Kerns, E. H.; Fan, K.; McConnell, O. J.; Carter, G. T. *Eur. J. Med. Chem.* **2003**, *38*, 223–232.
- (35) Avdeef, A.; Bendels, S.; Di, L.; Faller, B.; Kansy, M.; Sugano, K.; Yamauchi, Y. *J. Pharm. Sci.* **2007**, *96*, 2893–2909.
- (36) Vivekanandan, S.; Brender, J. R.; Lee, S. Y.; Ramamoorthy, A. *Biochem. Biophys. Res. Commun.* **2011**, *411*, 312–316.
- (37) Hou, L.; Shao, H.; Zhang, Y.; Li, H.; Menon, N. K.; Neuhaus, E. B.; Brewer, J. M.; Byeon, I.-J. L.; Ray, D. G.; Vitek, M. P.; Iwashita, T.; Makula, R. A.; Przybyla, A. B.; Zagorski, M. G. *J. Am. Chem. Soc.* **2004**, *126*, 1992–2005.
- (38) Mayer, M.; Meyer, B. *J. Am. Chem. Soc.* **2001**, *123*, 6108–6117.
- (39) Wyttenbach, T.; Bowers, M. T. *Modern Mass Spectrometry, Topics in Current Chemistry*; Christoph, A. Schalley, Ed.; Springer: Berlin, 2003; 225, 207–232.
- (40) Bernstein, S. L.; Wyttenbach, T.; Baumketner, A.; Shea, J.-E.; Bitan, G.; Teplow, D. B.; Bowers, M. T. *J. Am. Chem. Soc.* **2005**, *127*, 2075–2084.
- (41) Bernstein, S. L.; Dupuis, N. F.; Lazo, N. D.; Wyttenbach, T.; Condron, M. M.; Bitan, G.; Teplow, D. B.; Shea, J.-E.; Ruotolo, B. T.; Robinson, C. V.; Bowers, M. T. *Nat. Chem.* **2009**, *1*, 326–331.
- (42) Gessel, M. M.; Wu, C.; Li, H.; Bitan, G.; Shea, J.-E.; Bowers, M. T. *Biochemistry* **2012**, *51*, 108–117.
- (43) Zheng, X.; Gessel, M. M.; Wisniewski, M. L.; Viswanathan, K.; Wright, D. L.; Bahr, B. A.; Bowers, M. T. *J. Biol. Chem.* **2012**, *287*, 6084–6088.
- (44) Lesné, S.; Koh, M. T.; Kotilinek, L.; Kaye, R.; Glabe, C. G.; Yang, A.; Gallagher, M.; Ash, K. H. *Nature* **2006**, *440*, 352–357.
- (45) Upon 24 h incubation of Cu(II)-treated A $\beta$ 42 with ML, small sized A $\beta$  species disappeared.
- (46) Thinakaran, G.; Teplow, D. B.; Siman, R.; Greenberg, B.; Sisodia, S. S. *J. Biol. Chem.* **1996**, *271*, 9390–9397.
- (47) The concentration of ML with and without metal ions used for Figure 5a is relatively nontoxic in both N2a and N2aAPP<sub>swe</sub> cells (ca. 85% cell survival for 24 h; Supporting Information Figure S12). The concentrations (0 to 10  $\mu$ M) of ML, which do not interfere with the analysis of MTT assay, were selected for cell studies.
- (48) Charkoudian, L. K.; Pham, D. M.; Franz, K. J. *J. Am. Chem. Soc.* **2006**, *128*, 12424–12425.
- (49) Re, R.; Pellegrini, N.; Proteggente, A.; Pannala, A.; Yang, M.; Rice-Evans, C. *Free Radical Biol. Med.* **1999**, *26*, 1231–1237.
- (50) Schugar, H.; Green, D. E.; Bowen, M. L.; Scott, L. E.; Storr, T.; Böhmerle, K.; Thomas, F.; Allen, D. D.; Lockman, P. R.; Merkel, M.; Thompson, K. H.; Orvig, C. *Angew. Chem., Int. Ed.* **2007**, *46*, 1716–1718.
- (51) *BBB Protocol and Test Compounds*; pION Inc.: Woburn, MA, 2009.
- (52) Due to limited stability of ML, confirmed employing human, rat, and mouse liver microsomes (half time ( $t_{1/2}$ ) < 30 min, susceptible to metabolism in liver microsomes; [ML] = 1  $\mu$ M, 37 °C, ketanserin as a reference compound; this in vitro metabolic stability study was performed by a Contract Research Organization, Shanghai Chem-Partner Co., Ltd.), the brain and plasma concentrations were measured at a short incubation time point (i.e., 5 min).
- (53) Roth, R.; Erlenmeyer, H. *Helv. Chim. Acta* **1954**, *37*, 1064–1068.
- (54) Waibel, M.; Hasserodt, J. *Tetrahedron Lett.* **2009**, *50*, 2767–2769.
- (55) Pringle, S. D.; Giles, K.; Wildgoose, J. L.; Williams, J. P.; Slade, S. E.; Thalassinou, K.; Bateman, R. H.; Bowers, M. T.; Scrivens, J. H. *Int. J. Mass Spectrom.* **2007**, *261*, 1–12.
- (56) Wyttenbach, T.; Kemper, P. R.; Bowers, M. T. *Int. J. Mass Spectrom.* **2001**, *212*, 13–23.
- (57) Gidden, J.; Baker, E. S.; Ferzoco, A.; Bowers, M. T. *Int. J. Mass Spectrom.* **2005**, *240*, 183–193.
- (58) Mason, E. A.; McDaniel, E. W. *Transport Properties of Ions in Gases*; Wiley: New York, 1988.

- (59) Schanda, P.; Brutscher, B. *J. Am. Chem. Soc.* **2005**, *127*, 8014–8015.
- (60) Glasoe, P. K.; Long, F. A. *J. Phys. Chem.* **1960**, *64*, 188–190.
- (61) Yoo, S. I.; Yang, M.; Brender, J. R.; Vivekanandan, S.; Sun, K.; Joo, N. E.; Jeong, S.-H.; Ramamoorthy, A.; Kotov, N. A. *Angew. Chem., Int. Ed.* **2011**, *50*, 5110–5115.
- (62) Fawzi, N. L.; Ying, J.; Torchia, D. A.; Clore, G. M. *J. Am. Chem. Soc.* **2010**, *132*, 9948–9951.
- (63) Soong, R.; Brender, J. R.; Macdonald, P. M.; Ramamoorthy, A. *J. Am. Chem. Soc.* **2009**, *131*, 7079–7085.
- (64) Huang, R.; Vivekanandan, S.; Brender, J. R.; Abe, Y.; Naito, A.; Ramamoorthy, A. *J. Mol. Biol.* **2012**, *416*, 108–120.
- (65) Narayanan, S.; Reif, B. *Biochemistry* **2005**, *44*, 1444–1452.
- (66) Airoidi, C.; Sironi, E.; Dias, C.; Marcelo, F.; Martins, A.; Rauter, A. P.; Nicotra, F.; Jimenez-Barbero, J. *Chem. Asian J.* **2013**, *8*, 596–602.
- (67) Laurents, D. V.; Gorman, P. M.; Guo, M.; Rico, M.; Chakrabartty, A.; Bruix, M. *J. Biol. Chem.* **2005**, *280*, 3675–3685.
- (68) Morris, G. M.; Huey, R.; Lindstrom, W.; Sanner, M. F.; Belew, R. K.; Goodsell, D. S.; Olson, A. J. *J. Comput. Chem.* **2009**, *30*, 2785–2791.
- (69) Petkova, A. T.; Yau, W.-M.; Tycko, R. *Biochemistry* **2006**, *45*, 498–512.
- (70) Schüttelkopf, A. W.; van Aalten, D. M. F. *Acta Crystallogr., Sect. D: Biol. Crystallogr.* **2004**, *60*, 1355–1363.
- (71) Singh, U. C.; Kollman, P. A. *J. Comput. Chem.* **1984**, *5*, 129–145.
- (72) Gasteiger, J.; Marsili, M. *Tetrahedron* **1980**, *36*, 3219–3228.
- (73) Gasteiger, J.; Marsili, M. *Tetrahedron Lett.* **1978**, *19*, 3181–3184.
- (74) Morris, G. M.; Goodsell, D. S.; Halliday, R. S.; Huey, R.; Hart, W. E.; Belew, R. K.; Olson, A. J. *J. Comput. Chem.* **1998**, *19*, 1639–1662.
- (75) Gans, P.; Sabatini, A.; Vacca, A. *Ann. Chim.* **1999**, *89*, 45–49.
- (76) Alderighi, L.; Gans, P.; Ienco, A.; Peters, D.; Sabatini, A.; Vacca, A. *Coord. Chem. Rev.* **1999**, *184*, 311–318.
- (77) Mancino, A. M.; Hindo, S. S.; Kochi, A.; Lim, M. H. *Inorg. Chem.* **2009**, *48*, 9596–9598.
- (78) Spencer, V. A.; Sun, J.-M.; Li, L.; Davie, J. R. *Methods* **2003**, *31*, 67–75.